HIGH-FREQUENCY BULK WAVE MEASUREMENTS OF STRUCTURAL CERAMICS

C. H. Chou, B. T. Khuri-Yakub, K. Liang and G. S. Kino
Stanford University
Stanford, CA. 94305

ABSTRACT

A 50 MHz C-scan imaging system is under construction for fast defect detection. A high-frequency (150-450 MHz) A-scan system is used for host material evaluation, and defect characterization. Several signal processing schemes such as time and space averaging, Wiener filtering, diffraction and propagation loss corrections are used in the process of defect characterization. Further modifications of the exact theory of scattering from spherical inclusions are made to ease the process of defect identification.

C-SCAN SYSTEM

A C-scan imaging system is being built to scan ceramics for interior defects. Initially, the device will operate at 50 MHz with a partially focused transducer to produce a beam approximately 1 mm in diameter. The device will be capable of scanning in both the x and y directions along the surface of a ceramic. By operating in a reflection mode, it should be possible to determine both the depth and the transverse position of a flaw. Eventually, it is intended to operate at frequencies as high as 400 MHz and to use the same system to evaluate the size and nature of the flaw. By using a moveable point source as a synthetic aperture system, i.e., a focused beam focused on the surface of the ceramic, we expect eventually to be able to reconstruct an image of the flaw on the computer.

The mechanically-scanned system being designed for this purpose has to satisfy the following requirements:

(1) the system should be computer compatible, and it should be possible to control the whole system operation from a computer terminal; and

(2) the mechanical scans should be accurate to about 10 μm or less (.1λ at 100 MHz).

Thus, defect location and evaluation could be eventually carried out on one system. We believe that such a system will combine the advantages of A-scan with those of the acoustic microscope, but be able to examine internal as well as surface defects. For this application, steps of the order of one or two wavelengths in the X and Y directions are usually required.

System Design - The system has been designed to operate in one or any combination of the following modes:

Slew Mode - Scanning is at constant velocity. The maximum scan velocity is 5 cm/sec set by thumb-wheel switches.

Increment Mode - Scanning is carried out by stepping from one point to the next. The step size can be varied from 50 μm to 1 cm with an accuracy of ±8μm . The mechanical settling time per step is 3 msec . In this mode, the number of rf samples taken per step is settable from 0-999 . The speed of the scan is controlled by the operator.

Go-To Mode - In this mode, the transducer can be moved to any location of interest in its field. The position is dialed on thumb-wheel switches and is found with an accuracy of ±8μm . The scan can be continued from this location in any of the modes previously described.

Flag-Stop Mode - In this mode, the scan stops when a defect is located. A discriminator set by thumb-wheel switches is used to decide at what level a signal is considered to be due to a defect. The discriminator also gives out a signal to drive the Z-axis (pen up, pen down) of an X-Y recorder.

A combination of these modes of operation may be the best way to use the system. For instance, a slew scan at a moderate speed can be used to determine the rough location of the defects. A go-to command followed by a fine-step scan is used to determine the correct location of the defect. A flag-stop can be used to stop the scan over the defect location (when the signal is maximum). The X-Y location of the defect is displayed on digital displays in the main panel and/or the plot of an X-Y recorder. The A-scan display is continuously monitored on a cathode ray oscilloscope which can be used to determine the location of the defect in the depth of the sample.

HIGH-FREQUENCY A-SCAN SYSTEM

A schematic diagram of the A-scan system used in our study is shown in Fig. 1. The bottom end of the buffer rod is polished with a radius of curvature of 20 cm . Contact to the ceramic under study is made by pushing the curved end of the buffer rod against the ceramic without using a contacting layer such as gold. The transducer is excited with a 30 V , 2 nsec electric pulse in order to obtain broad bandwidth operation (150-450 MHz).[1]

The received signal at the transducer is passed into a sampling oscilloscope which yields an output that is a slowed down version of the pulse. A Biomation analog-to-digital converter digitizes the slowed down pulse for insertion into a PDP 11-34 minicomputer. The computer is used to take fast Fourier transforms and correct the received signal.[2]

Signal Processing Methods - The signal processing schemes we use to correct and improve the signals from the defects are:

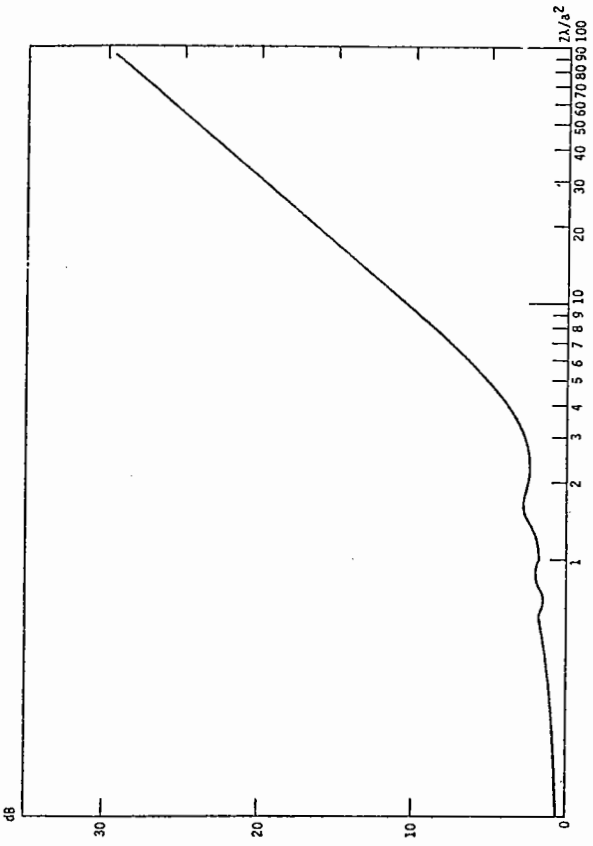

Fig. 1. Loss of power due to diffraction between two identical piston transducers of radius a as a function of their distance apart in units of a^2/λ .

1. Time domain averaging.
2. Space domain averaging.
3. Wiener filtering.
4. Propagation loss correction.
5. Diffraction loss correction.

Time domain averaging consists of reading the signal N times at a certain location, then taking the average of the sum of the N signals. The amplitude of the signal from a defect relative to random noise is improved by $\sqrt{N}$. Space domain averaging consists of reading the signal at N different locations on the sample, then taking the average of the N signals. The criteria for the maximum step over the sample is to keep the signal from a defect almost constant, i.e., the defect is kept within the radius of the beam. This type of averaging improves the signal-to-grain scattering noise level.[3] Wiener filtering is a deconvolution scheme used to remove the effect of the transducer response. This technique, which has been described in the previous report, consists mainly of dividing the received signal by the impulse response of the transducer while taking account of the presence of noise in the system.[1] Propagation and diffraction loss corrections take care of acoustic beam spreading and propagation loss through the host material itself. By using the techniques described, we have been able to improve the signal-to-noise ratio in the system, and look at the impulse response of defects separated from the effect of the transducer and the propagation media.

Propagation Loss Measurements - One important step in the NDE of ceramics is to evaluate the quality of the host material itself. If the host material is porous or has large grains and does not meet fracture strength requirements, there is no point in looking for isolated defects and attempting to characterize them. For this test, we carry out a propagation loss measurement vs. frequency, as described in an earlier publication.[4]

The most important development in the last year has been to calculate the exact diffraction loss for all ranges of normalized distances from the transducer. This loss can be written as

$$\frac{\langle p \rangle}{\langle p_0 \rangle} = 2e^{-jkz} \int_0^\infty \frac{J_1^2(y)}{y} e^{jS^2 y/4\pi} dy \qquad (1)$$

where $\langle p \rangle$, $\langle p_0 \rangle$ are the average values of the pressure over the area of the output transducer at a distance z , and at the input transducer, respectively. $S = z/a^2$ where a is the transducer radius, k is the wave number, and $J_1(y)$ is a Bessel function of the first kind and first order.

The diffraction loss L is therefore

$$L = 20 \log \frac{\langle p \rangle}{\langle p_0 \rangle} \qquad (2)$$

Fig. 1 shows a plot of the diffraction loss versus S , for S varying from 1 to 100 . When the medium is anisotropic, the loss can be found simply by changing S to $(1 - 2b)S$ where b is an anisotropy coefficient defined as

$$b = \frac{(C_{33} - C_{13} - 2C_{44})(C_{33} + C_{13})}{2C_{33}(C_{33} - C_{44})} \qquad (3)$$

For a material with hexagonal symmetry,[5] such as sapphire (the buffer rod), b = .16 . For isotropic materials, these formulae are reliable for $S \ll 1$, provided $ka \gg 10$. For anisotropic materials, however, the accuracy of the formula is better for $S > 1$.

We repeated our measurements of propagation loss in hot pressed NC 132 silicon carbide and at different locations in the same sample. Fig. 2 shows the results of some of these measurements. The loss is about 3 dB/cm at 300 MHz and follows an f^4 dependence, as would be expected from Rayleigh scattering theory. The value of the propagation loss at 300 MHz and the f^4 dependence were consistent for good hot-pressed silicon nitride samples. In a later section, we will discuss our results on some "bad" or lossy samples. It will be noted that, especially in the lower frequency range, it is vital to correct for diffraction.

Scattering Theory - The type and size of defects is determined by comparing their back-scattered power spectra to theory. The theoretical calculations for various types of spherical inclusions in a silicon nitride host matrix were calculated using the theory developed by Ying and Truell,[6] and Johnson and Truell,[7] using techniques similar to those of Richardson and Cohen.[8] A PDP 11-34 minicomputer was used to carry out the calculations.

We found that the time taken to calculate the back-scattered signal versus ka (where $k = 2\pi/\lambda$, and a is the radius of the defect) took about 8 min for $9 < ka < 20$. For $0 < ka < 100$, the time taken per inclusion was roughly about 1 hr. The results for such calculations are shown in Figs. 3a, b, and c.

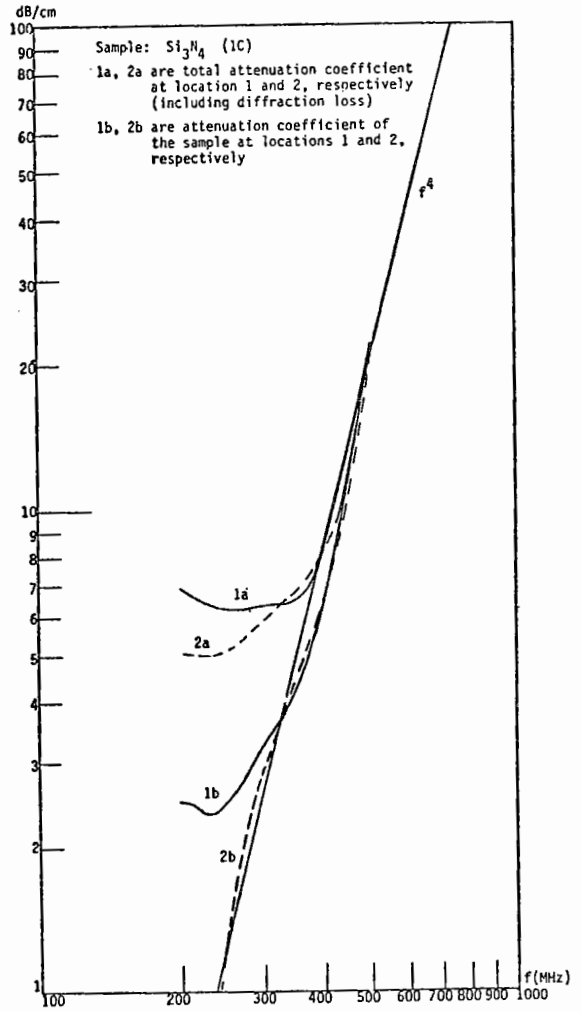

Fig. 2. Attenuation measurement at two different locations.

It is convenient to plot the theoretical scattering versus $\log ka = \log k + \log a$. Then, if a is unknown, as it would be in an experiment, the comparison between theory and experiment can be made by directly overlapping the experimental and theoretical curves, and finding a from the position where they overlap.

It will be noted that the scattering signal variation with frequency, denoted by the full line curves, is much simpler in form for a vacancy than for an inclusion. The reason is that the inclusion has associated with it several types of resonances. Put another way, the vacancy gives rise to a back-scattered echo from its front surface, and a wave which can propagate around the surface and interefere with the echo from the front surface, thus giving rise to the quasi-periodic back-scattering structure. On the other hand, a wave can propagate through the middle of the inclusion and be scattered from its back surface as either a shear or a longitudinal wave. The return echoes interfere with each other, thus giving rise to a far more complicated form for the scattering cross-section as a function of frequency.

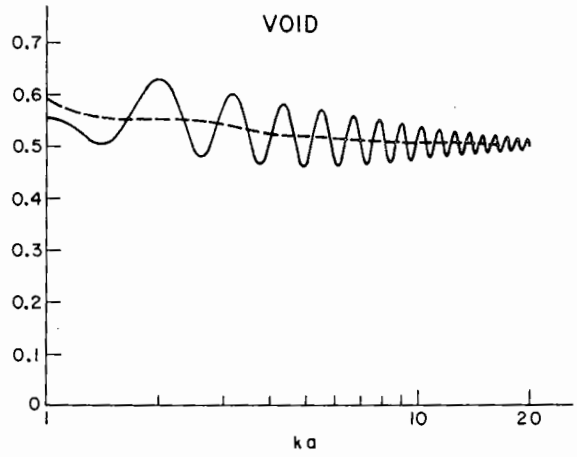

Fig. 3a. The scattering cross-section σ from a void in Si_3N_4 as a function of ka.

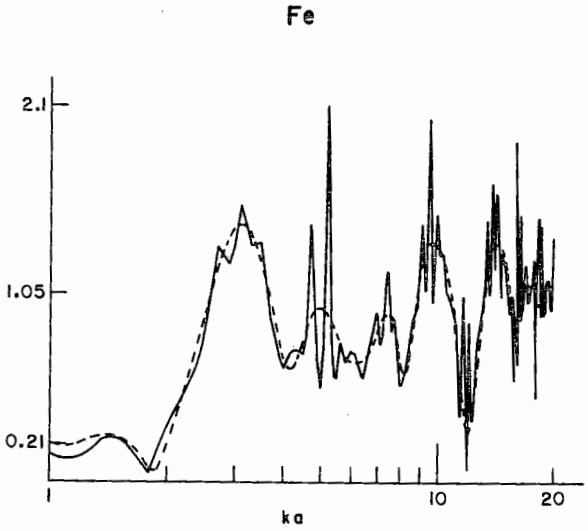

Fig. 3b. The scattering cross-section σ for Si_3N_4 as a function of ka.

The time domain impulse response of the defects has been calculated by inverse Fourier transforming the calculations of Fig. 3 into the time domain. A cosine squared window centered at ka = 10 and equal to zero at ka = 0 and ka = 20 was multiplied by the frequency response before inverse Fourier transforming in order to limit the time domain response, and give the pulses a shape like a real transducer response. The results of the calculations are shown in Figs. 4a, b, and c.

By examining the time domain responses in detail, it is possible to compare the results with simple optical ray tracing concepts, and determine the types of waves that contribute to the

impulse responses of the defects.[9] The various waves are shown schematically in Fig. 4. It is obvious from Figs. 3 and 4 that different inclusions give rise to different return echo responses in both the frequency and time domains, thus making it possible to differentiate between different types of defects. It is also obvious that a void can be directly differentiated from inclusions because its spectrum is very flat with frequency, i.e., there is only a strong return echo from its front surface. Thus, it is simple to classify defects as to whether they are voids or inclusions.

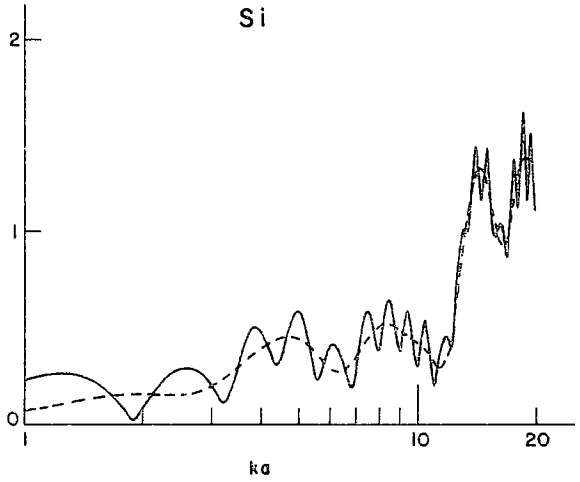

Fig. 3c. The scattering cross-section σ from Si in Si_3N_4 as a function of ka .

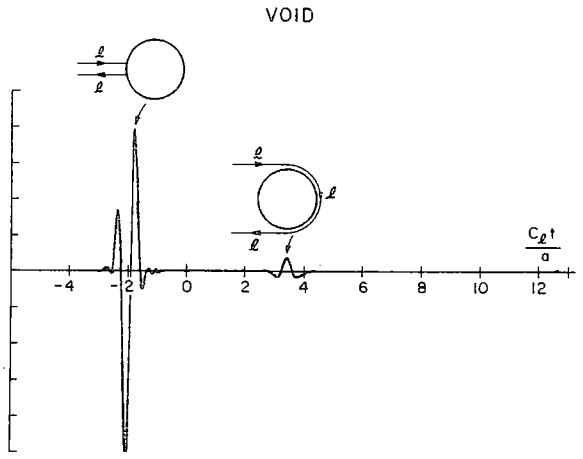

Fig. 4a. Relative scattering cross-section from a void as a function of time.

If a defect is a void, it is typically not possible to detect the second echo due to the leaky wave propagating around it. This we believe is due to the fact that the inside surface of the void is rough and scatters the circumferential wave before it reaches the transducer. The size of a void is then determined from a measurement of the echo amplitude. Another distinction to be made is whether a void is a "volumetric" void or a flat crack. This is typically done by measuring the thickness of the void either by measuring its location from the two sides of the sample, or by measuring the distance from the back wall to the mirror image of the defect with respect to the back wall.

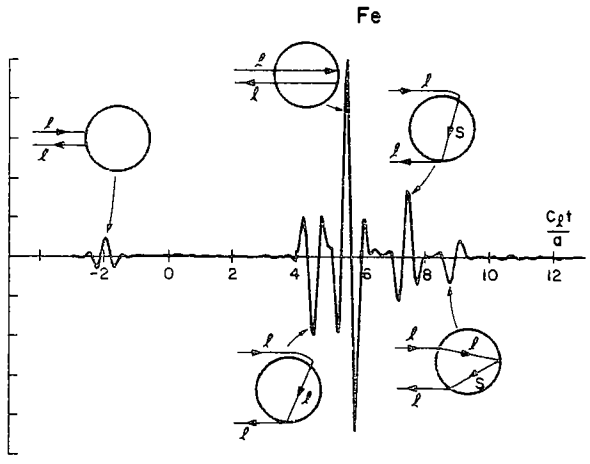

Fig. 4b. Relative scattering cross-section from Fe as a function of time.

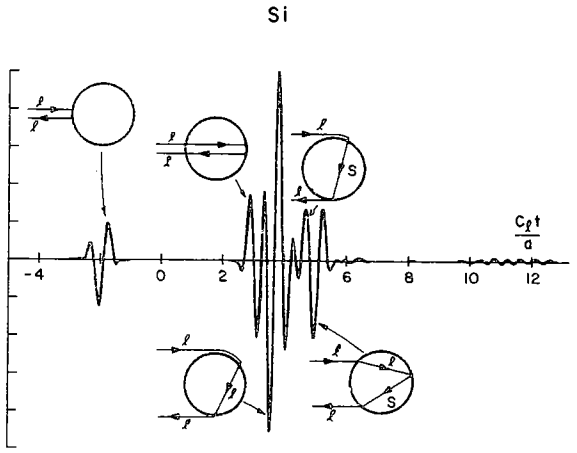

Fig. 4c. Relative scattering cross-section from Si as a function of time.

If the defect is an inclusion, we may use the signal processing schemes described above to compare the back-scattered spectrum of the flaw to theory and decide on its type and size. In our efforts to confirm the theory with samples having seeded defects, a new problem arose: the seeded samples are usually porous resulting in a large amount of back-scattering from grain boundaries and, of course, a large amount of propagation loss in certain cases. The effect of this grain scattering is that the resultant noisy signal tends to obscure the front face echo, which is relatively weak compared to the back face echo. In some cases space averaging enabled us to reduce the effect of grain scattering and isolate the front face echo. In many other cases, this was not possible, and we had to decide on the type and size of inclusions using the defect back-face echoes only.

We simulate this case in the theory by gating out the specular reflection from the front face in

the time domain, then Fourier transforming the remainder of the signal into the frequency domain. The results of this calculation are shown as dashed lines in Figs. 3a, b and c. Notice that as there is no longer interference between the back-face and front-face echoes, the high-frequency ripples (as a function of ka) are removed. The modified spectra differ for each material, and so allow flaw identification.

Results - We used a number of seeded NC 132 silicon nitride disks to confirm our theory on detection and characterization of defects. The samples were seeded with iron (Fe), silicon (Si) and carbon (C) inclusions. The sizes of the inclusions were either 100 μm or 400 μm in diameter. We tested seven of these samples and the results are shown in Table I.

	Type & Size of Seeded Defect	ρ kg/m^3	v_1 km/sec	α dB/cm 300 MHz	No. of Defects	No. of Voids	No. of Cracks	# and Size of Identified Inclusions	No. of Unidentified Inclusions	Remarks
67	C-400 μm	3.13	10.13	25	5	2	1	0	2	30 dB Inhomogeneous
86	Fe-400 μm	3.2	10.3	12	3	0	2	1 Fe	0	7dB Inhomogeneous
93	Si-400 μm	2.95	9.24	80	2	0	1	1 Si	0	>30 dB Inhomogeneous
27	C-100 μm	3.24	10.8	7	18	9	6	0	3	Very Porous
1	Si-100 μm	3.23	10.7	11	10	1	4	3 Si 100 μm	2	---
2	Fe-100 μm	3.28	10.9	9	23	0	20	1 Fe	2	High Density of Small Cracks
73	C-400 μm	3.21	10.62	6	4	0	4	0	0	---

Measured Parameters

TABLE I

Results of measurements carried out on various Si_3N_4 samples.

From Table I, the following conclusions can be made.

Some of the samples exhibited a large amount of localized inhomogeneity. In sample #67, the echo from the back side of the sample changed by 30 dB when the transducer was moved from one location to another, 1 or 2 mm away.

The density of the samples varied dramatically from one to the other. Sample #93 had a 10% lower density than fully dense silicon nitride. The densities of the rest of the samples are also lower by lesser amounts.

The longitudinal wave velocity measured at a frequency of 300 MHz is lower than expected for fully dense silicon nitride (11.0 km/sec). The longitudinal wave velocity seems to roughly be proportional to the density of the material. This indicates that the stiffness of the material decreases dramatically when the density decreases. The estimated stiffness of sample #93 is 36% lower than theoretically predicted for fully dense silicon nitride (NC 132).

The propagation loss measurement ties in very well with the density and longitudinal velocity measurements. We note that the less dense and correspondingly slower velocity materials have more propagation loss due to scattering from pores in the samples. From these results, we can clearly conclude that measurements of density, velocity, and propagation loss give direction information on the quality of the material and could be used to improve the manufacturing process before proceeding to look for isolated defects.

Many isolated defects were found in the samples tested. In sample #2, 23 defects were found in an area of only 2mm x 3mm . In the lossy, inhomogeneous samples (#67, 86 and 93), far fewer defects were found because of the excessive propagation loss. This limits our sensitivity and obscures the back-scattered signal from defects in the back-scatter signal from the pores. In all the samples tested, a large amount of scattering from porosity was observed. The level of this scattering was comparable in amplitude to the reflection from the front side of the inclusions. Using the processing schemes described previously, we were able to separate the front face echo of the defect, and thus decide on its type and size, as tabulated. In other cases, we were able to decide on the type and size of an inclusion without using the front-face echo, as we have described. However, there were still some inclusions that we could not identify because of the large amount of scattering from porosity.

Judging by the number of defects found in the seeded samples, we observe that over 90% of all defects found were either voids or appeared to be cracks, which in fact were later found to be BN discs. Thus, many voids may not occur in unseeded samples and certainly do not in high quality NC 132 material.

We concentrated our detailed quantitative interpretation on the measurements of sample #1, the sample with isolated inclusions. After processing all the signals from the defects, as described, we found that three of the defects in the sample were Si inclusions 100 μm in diameter. This result is in good agreement with the type and size of inclusions with which the sample was said to be seeded.

At the time of writing, the sample had been partially polished to the locations of some of the defects we found. The results indicate that we were able to detect every defect present in the portion of the sample examined. Moreover, all the cracks we detected were found at the prescribed locations. They were in reality thin disks of BN , a material used in the pressing operation, which is relatively harmless as far as its effect on fracture is concerned. Flat empty cracks do not occur in hot pressed Si_3N_4 , and hence when "cracks" are detected by our acoustic method, they must be expected to be thin disks filled with a low acoustic impedance material such as BN . Hence, for hot pressed Si_3N_4 , all the detected cracks are thin disks of BN .

In another example, we decided that one of the voids we detected was actually two voids separated by 50 μm in depth. This decision was made because two echoes of equal amplitude were detected with ~10 nsec separation in time. The actual defect is shown in Fig. 5a. The defects consist of two voids, as predicted, the two voids being connected by a porous region.

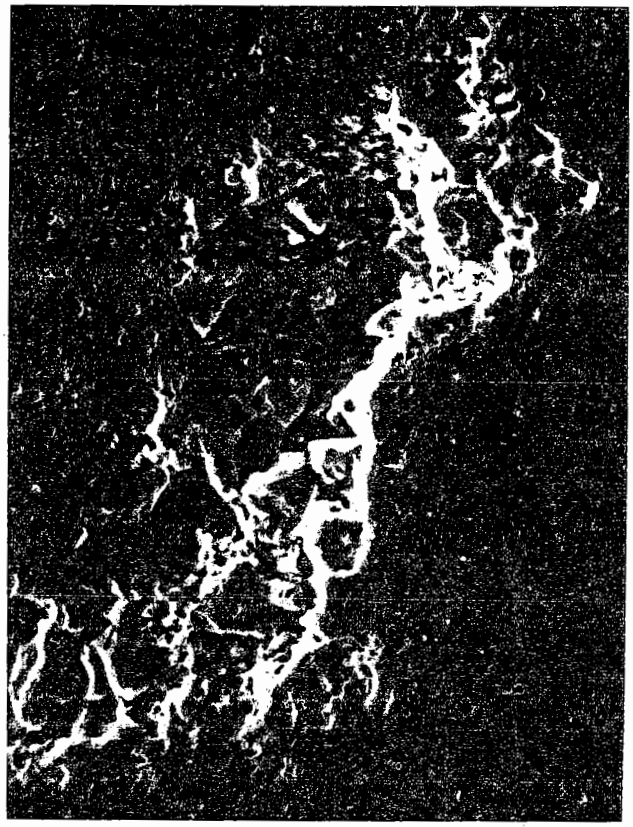

Fig. 5a. S.E.M. picture of two voids, 50 μ apart.

Fig. 5b. S.E.M. picture of MgO rich defect region.

Some of the defects detected were of a new and unexpected type. They corresponded to a series of echoes with a short time separation between them (10-15 nsec), as would be expected from granular scattering. One such defect is shown in Fig. 5b. This defect turned out to consist of regions of concentrated MgO inclusions, a material used in the hot pressing operation to increase the density of the ceramic. It was thought that this material would disperse and not give rise to any problems; however, it obviously does not always do so. This unexpected defect, which was first detected clearly by acoustic techniques, is likely to have an important effect on the fracture characteristics of these ceramics.

There are a few more defects present in the samples, namely Si . We are presently awaiting the results of the polishing to compare with our acoustic measurements. At the present time, the polishing process has reached only one defect. The results obtained on this one defect are not encouraging, because the Si seed turned out to be porous, and of a larger size than had been predicted by our theory. This would be expected because the theory was based on the supposition that the defect was a sphere of Si . Here it was not spherical, nor was it pure Si . It remains to be seen whether the other Si seeds have changed in the same way.

CONCLUSIONS

We have developed two systems to locate and characterize defects in ceramics. We have used a set of signal processing schemes to improve the signal-to-noise (electronic noise and grain-scattering noise) ratio and to correct the signals received from defects. We believe that our theoretical and experimental techniques have not been fully tested yet, because the seeded samples we had were inferior to hot pressed, unseeded silicon nitride. However, we feel confident that our technique will work well on high quality samples of the type that should be used in real turbines. One difficulty is that artificially seeded materials always appear to be far worse in quality than the natural unseeded samples with naturally occuring defects present.

It appears from our initial results that the seeded defects which occur are not always spherical or simple in nature. This presumably will be the case with naturally occuring defects. Thus, although there are acoustic signatures associated with the different types of defects that are present, it will be necessary to develop further acoustic methods to provide a complete unequivocal quantitative identification of the size and type of all defects present. Naturally occuring inclusions of biphase materials of awkward shape are the most difficult to identify. For a complete analysis, it will probably be necessary to resort to the imaging techniques which we are presently developing.

REFERENCES

1. B. T. Khuri-Yakub, G. S. Kino, A.P.L., Vol. 31, No. 2 (15 Jan. 1977).

2. Y, Murakami, B. T. Khuri-Yakub, G. S. Kino, J. M. Richardson, A. G. Evans, A.P.L., Vol. 33, No. 8 (15 Oct. 1978).

3. K. Goebbels, P. Höller, Proceedings of the First International Symposium on Ultrasonic Material Characterization, Gaithersburg, Md., June, 1978.

4. A. G. Evans, B. R. Tittmann, L. Ahlberg, B. T. Khuri-Yakub, G. S. Kino, J.A.P., Vol. 49, No. 5, May, 1978.

5. P. C. Waterman, Phys. Rev. 113, 1240 (1959).

6. C. F. Ying, R. Truell, J. Appl. Phys, 27, 1086 (1956).

7. G. Johnson, R. Truell, J. Appl. Phys., 36, 3466 (1965).

8. J. M. Richardson, D. Cohen, Rockwell Science Center (Private Communication).

9. Y. H. Pao, W. Sachse, J. Acoust. Soc. Am. Vol. 56, No. 5, Nov. 1974.

ACKNOWLEDGMENT

This work was supported by the Advanced Research Projects Agency under Rockwell International subcontract RI74-20773.

SUMMARY DISCUSSION
(P. Khuri-Yakub)

Wolfgang Sachse (Cornell University): One comment and a question. It's nice to see that someone else has found Weibull useful for classifying certain defects, but my question is: you said you made the diffraction correction. You mean to say that you found what is the diffraction of a sound wave as it leaves the buffer rod into the sample?

P. Khuri-Yakub: No. When you want to make a correction loss, if you're at high TS, and if you look at all the published data, you find it goes up to four or five.

Wolfgang Sachse: That's for a piston radiator?

P. Khuri-Yakub: That is a piston transducer, too.

Wolfgang Sachse: I'm not sure, but anyhow --

P. Khuri-Yakub: We just took it farther because we needed to get that right correction there.

Jim Rose (Univ. of Michigan): You cut off your theory of KA of 1. Does that imply in your data analysis you don't use the low-frequency information?

P. Khuri-Yakub: It depends on the size of the transducer (inaudible), the only reason why we did that was because we plotted on a log-log scale (inaudible).

# #